

Phonon, Two-Magnon and Electronic Raman Scattering of $\text{Fe}_{1+y}\text{Te}_{1-x}\text{Se}_x$

K. Okazaki^{1,4,*}, S. Sugai^{1,4}, S. Niitaka^{2,4}, and H. Takagi^{2,3,4}

¹*Department of Physics, Nagoya University, Nagoya, Aichi 464-8602, Japan*

²*RIKEN (The Institute of Physical and Chemical Research), Wako, Saitama 351-0198, Japan*

³*Department of Advanced Materials Science, University of Tokyo, Kashiwa, Chiba 277-8581, Japan*

⁴*JST, Transformative Research-Project on Iron Pnictides (TRIP), Chiyoda-Ku, Tokyo 102-0075, Japan*

(Dated: January 17, 2022)

We have measured Raman scattering spectra of single-crystalline $\text{FeTe}_{0.6}\text{Se}_{0.4}$ ($T_c \sim 14.5$ K) and its parent compound $\text{Fe}_{1.074}\text{Te}$ at various temperatures. In the parent compound $\text{Fe}_{1.074}\text{Te}$, A_{1g} and B_{1g} modes have been observed at 157.5 and 202.3 cm^{-1} , respectively, at 5 K. These frequencies qualitatively agree with the calculated results. Two-magnon excitation has been observed around 2300 cm^{-1} for both compounds. Temperature dependence between the electronic Raman spectra below and above T_c has been observed and 2Δ and $2\Delta/k_B T_C$ have been estimated as 5.0 meV and 4.0, respectively.

PACS numbers: 74.25.nd, 74.25.nd, 74.25.Kc, 63.20.D-, 74.25.Ha

I. INTRODUCTION

Since the discovery of superconductivity in $\text{LaFeAsO}_{1-y}\text{F}_y$ (1111 system) with $T_c = 26$ K,¹ extensive researches have been devoted to the iron-based superconductors. Immediately after the discovery, T_c enhancement of $\text{LaFeAsO}_{1-y}\text{F}_y$ under high-pressure upto ~ 43 K² and higher T_c (~ 55 K) of $\text{SmFeAsO}_{1-y}\text{F}_y$ ³ has been found. Up to now, various iron-based superconductors with the different crystal structures has been discovered such as $\text{Ba}_{1-x}\text{K}_x\text{Fe}_2\text{As}_2$ (122 system),^{4,5} LiFeAs (111 system),^{6,7} $\text{Fe}_{1+y}\text{Te}_{1-x}\text{Se}_x$ (11 system),⁸⁻¹⁰ $\text{Sr}_4\text{V}_2\text{O}_6\text{Fe}_2\text{As}_2$ (42622 system),¹¹ and so on. These iron-based superconductors commonly have FePn_4 (Pn : pnictogen) or FeCh_4 (Ch : chalcogen) tetragonal layers. In addition, there are some other common features in the iron-based superconductors, i.e., antiferromagnetic (AFM) ordering in the parent compound, nesting feature of the Fermi surfaces (FS), and so on. FS of these iron-based superconductors have been calculated on the basis of the density functional theory (DFT)¹²⁻¹⁵ and it has been pointed that hole FS around Γ point and electron FS around M point are nearly nested. This has been confirmed by the calculations of Lindhard response function.^{13,15-18} The importance of spin fluctuations due to the nesting feature of FS and a possibility of s_{\pm} superconducting-gap symmetry have been proposed.^{19,20} Experimentally, FS similar to the DFT results^{21,22} and AFM ordering in the parent compounds²³⁻²⁵ have been observed.

Superconductivity of 11 system has first discovered by Hsu *et al.*⁸ in FeSe with $T_c \sim 8$ K. T_c of substituted compounds reaches up to ~ 14 K at $x = 0.4$.¹⁰ Under hydrostatic pressure, T_c of Fe_{1+y}Se is enhanced to ~ 37 K around 7-9 GPa.^{26,27} Among the iron-based superconductors, 11 system has the simplest structure and consists of only FeCh_4 layer.²⁸ Hence, 11 system can be assumed to be suitable to reveal the relationship between the crystal structure and the origin of superconductivity. However, important differences between 11 system and

the other iron-arsenide superconductors should be noted, i.e., while the iron arsenide superconductors show single-stripe AFM ordering²³⁻²⁵ and those AFM wave vector $Q_{AF} = (\pi, \pi)$ coincide with the Γ - M nesting vector between the hole FS around Γ point and the electron FS around M point. However, Fe_{1+y}Te shows a double-stripe AFM ordering and its $Q_{AF} = (\delta\pi, 0)$ is rotated by 45° from the nesting vector.^{25,29} δ is tunable depending on the amount of the excess irons and can be incommensurate for the large y .²⁹ Hence, 11 system can be regarded as a counter example that the nesting condition is not crucial for the AFM ordering. Hence, we may have to reconsider the relationship between the superconductivity and the spin fluctuation. On the other hand, an inelastic neutron scattering (INS) measurement in $\text{FeTe}_{0.6}\text{Se}_{0.4}$ reveals a resonance feature below T_c with the excitation energy of 6.5 meV and the wave vector of (π, π) .³⁰ Since this wave vector corresponds to the nesting vector, there is a possibility that while the long range AFM ordering in the parent compound of 11 system is not related to the FS nesting, the spin fluctuation with the (π, π) nesting wave vector is crucial for the emergence of superconductivity.

In this paper, we have reported the phonon, two-magnon, and electronic Raman scattering of the 11 system $\text{Fe}_{1.074}\text{Te}$ and $\text{FeTe}_{0.6}\text{Se}_{0.4}$ at various temperatures. Because the parent compound $\text{Fe}_{1.074}\text{Te}$ has a simultaneous structural and magnetic transition, some anomaly around the transition temperature can be observed in the phonon and/or magnon Raman scattering. On the other hand, it is interesting that how the Se-substitution effects are observed in the two-magnon excitation of the parent AFM compound $\text{Fe}_{1.074}\text{Te}$. This could be an important clue to reveal the relationship between the magnetic fluctuations and superconductivity. From the electronic Raman spectra, the size and symmetry of the superconducting gap could be determined.

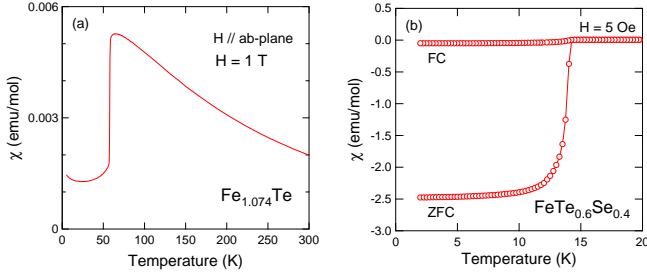


FIG. 1: (Color online) Results of magnetic measurements for (a) $\text{Fe}_{1.074}\text{Te}$ and (b) $\text{FeTe}_{0.6}\text{Se}_{0.4}$. T_s and T_c have been confirmed as ~ 58 K and 14.5 K, respectively.

II. EXPERIMENTAL

Single crystals of $\text{Fe}_{1+y}\text{Te}_{1-x}\text{Se}_x$ were grown by a melt-growth technique. Nominal compositions of the grown crystals were $\text{FeTe}_{0.9}$ and $\text{FeTe}_{0.5}\text{Se}_{0.5}$. The detailed procedures have been described in Ref. 31. The actual compositions were confirmed by the inductively coupled plasma (ICP) analysis as $\text{Fe}_{1.074}\text{Te}$ and $\text{FeTe}_{0.6}\text{Se}_{0.4}$, respectively. The structural and magnetic transition temperature T_s of the parent compound $\text{Fe}_{1.074}\text{Te}$ and the superconducting transition temperature T_c of $\text{FeTe}_{0.6}\text{Se}_{0.4}$ were confirmed by a superconducting quantum interference device (SQUID) magnetometer as shown in Fig. 1. T_s and T_c were ~ 58 K and 14.5 K, respectively. Raman-scattering spectra were measured with the fresh cleaved surfaces in a quasibackscattering configuration using a 5145 Å Ar ion laser, a triple monochromator, and a liquid-nitrogen-cooled CCD detector. The laser power was set to 20 mW and the laser spot was focused to $50 \times 500 \mu\text{m}^2$ on the sample surface. The wide-energy spectra were obtained by shifting the central wave number of the spectrometer. The obtained spectra were corrected for the efficiency of the spectrometer utilizing a standard lamp to keep the constant response for the light power. The polarization configuration is denoted by $k_i(E_i, E_s)k_s$, where $k_i(k_s)$ is the direction of the wave vector of incident (scattered) light and $E_i(E_s)$ is the polarization of the incident(scattered) light. The spectra were measured at four polarization configurations $c(aa)\bar{c}$, $c(ab)\bar{c}$, $c(xx)\bar{c}$, and $c(xy)\bar{c}$ in the ab -plane, where a and b denote the crystallographic a - and b -axis, respectively and x and y are the directions rotated by 45° from a -axis and b -axis in the ab -plane, respectively. The Raman active symmetries are $A_{1g} + B_{1g}$, B_{2g} , $A_{1g} + B_{2g}$, and B_{1g} for (aa) , (ab) , (xx) , and (xy) polarization configurations, respectively.

III. CALCULATION

We have also performed calculations of the phonon modes of FeSe and FeTe in a non-magnetic tetragonal

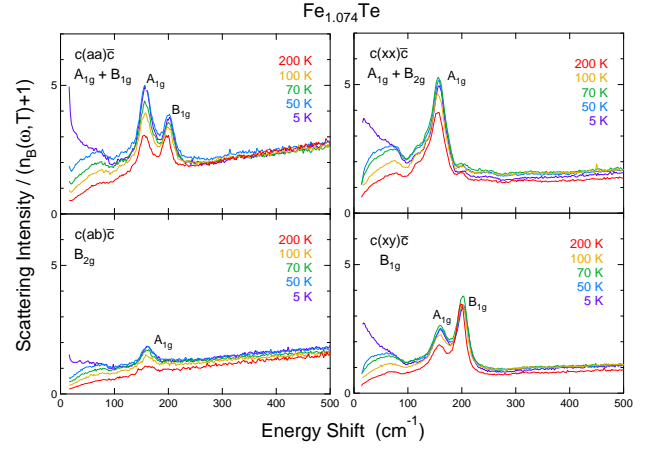


FIG. 2: (Color online) Temperature-dependent phonon Raman spectra of $\text{Fe}_{1.074}\text{Te}$. A_{1g} and B_{1g} modes have been observed at 157.5 cm^{-1} and 202.3 cm^{-1} , respectively, at 5 K.

phase in the framework of the density-functional perturbation theory based on the plane-wave basis method using the Quantum-Espresso code.³² The lattice parameters $a = 3.8097 \text{ Å}$ and $c = 6.2756 \text{ Å}$ for FeTe and $a = 3.7696 \text{ Å}$ and $c = 5.520 \text{ Å}$ for FeSe were used according to the X-ray diffraction measurements by Mizuguchi *et al.*³³ The internal parameter z corresponding to the chalcogen height from the iron plane was optimized via energy minimization. The optimized parameter z was 0.2507 for FeTe and 0.2343 for FeSe, respectively. These values are almost the same with the those used by Subedi *et al.*¹⁴ The cutoff energies were 50 Ry for the wavefunctions and 500 Ry for the electron density, respectively.

IV. RESULTS AND DISCUSSION

A. Phonon Raman Scattering

From the group theory considerations, Γ -point phonon modes of the tetragonal $\text{Fe}(\text{Te}, \text{Se})$ can be expressed as $\Gamma = A_{1g} + 2A_{2u} + B_{1g} + 2E_g + 2E_u$. While the Raman-active modes $\Gamma_{\text{Raman}} = A_{1g} + B_{1g} + 2E_g$, A_{1g} and B_{1g} modes can be observed in our measurements. Figure 2 shows phonon Raman spectra of $\text{Fe}_{1.074}\text{Te}$ in all the measured configurations. From the polarization dependence, we have concluded that A_{1g} and B_{1g} modes have been observed at 158 cm^{-1} and 202 cm^{-1} , respectively, at 5 K. Although A_{1g} mode should not be observed in the (ab) and (xy) configurations, this mode has been observed weakly also in those configurations. This should be due to the leakage of other polarization components. While the peak positions have slightly shifted to the higher energies with decreasing temperature, any distinct change has not been observed across the magnetic and structural transition temperature T_s . In other phonon Raman scattering measurements, Xia *et al.* have reported that A_{1g}

TABLE I: (Color online) The results of phonon-mode calculation and comparison with the Raman measurements

Symmetry	FeTe (cm^{-1})	FeSe (cm^{-1})	Expt. Fe _{1.074} Te	Atoms	Active
E_g	120.1	167.1		(Te,Se)	Raman
A_{1g}	168.4	221.9	158	(Te,Se)	Raman
B_{1g}	216.4	179.8	202	Fe	Raman
E_u	227.4	247.5		Fe+(Te,Se)	IR
E_g	274.1	313.0		Fe	Raman
A_{2u}	302.8	290.9		Fe+(Te,Se)	IR

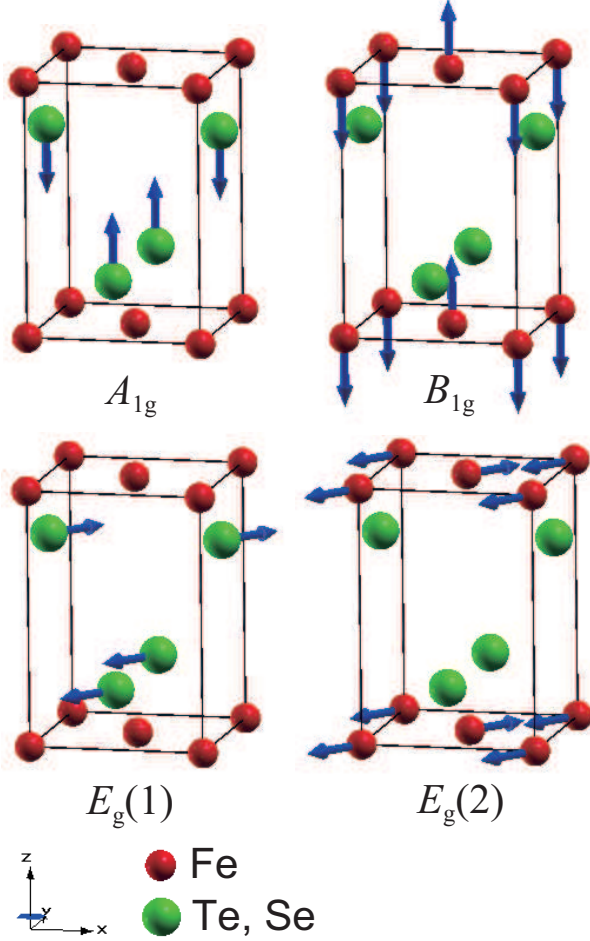


FIG. 3: (Color online) Atomic-displacement patterns of Raman active optical modes of Fe(Te,Se).

and B_{1g} modes are 159.1 cm^{-1} and 196.3 cm^{-1} , respectively, for single-crystal FeTe_{0.92}³⁴ and Kumar *et al.* have reported that those are 160 cm^{-1} and 224 cm^{-1} , respectively, for polycrystalline FeSe_{0.82}.³⁵

Table I shows a summary of the calculated results for the optical phonons of FeTe and FeSe. The irreducible representations, frequencies, main contribution of dis-

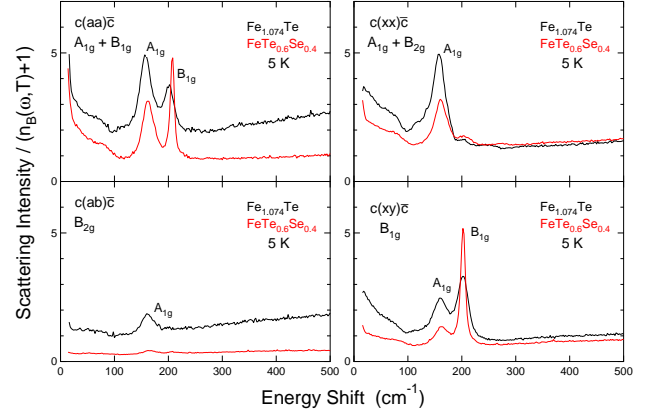


FIG. 4: (Color online) Comparison of phonon Raman spectra between the parent compound Fe_{1.074}Te and the superconducting FeTe_{0.6}Se_{0.4}. A_{1g} and B_{1g} modes of FeTe_{0.6}Se_{0.4} have been observed at 161 cm^{-1} and 202 cm^{-1} , respectively, at 5 K.

placed atoms, and activities have been listed. The experimental results of Fe_{1.074}Te also have been listed. The calculated frequencies of A_{1g} and B_{1g} modes of FeTe are qualitatively in accord with the the observed peak positions. The atomic displacement patterns of Raman-active modes are shown in Fig. 3. The observed A_{1g} and B_{1g} modes can be assigned to the c -axis anti-phase vibration modes of the chalcogens and the irons, respectively.

Figure 4 shows a comparison of phonon Raman spectra between the parent compound Fe_{1.074}Te and the superconducting FeTe_{0.6}Se_{0.4}. A_{1g} and B_{1g} modes of FeTe_{0.6}Se_{0.4} have been observed at 161 cm^{-1} and 202 cm^{-1} , respectively, at 5 K. Because B_{1g} mode is an iron vibration mode, this energy is almost the same between these two compounds. On the other hand, A_{1g} is a chalcogen vibration mode, this energy is slightly larger for FeTe_{0.6}Se_{0.4}. However, the energy difference of B_{1g} mode between Fe_{1.074}Te and FeTe_{0.6}Se_{0.4} seems to be too small as compared to the calculated results for FeTe and FeSe. This would be related to the facts that difference of the lattice constants between FeSe and substituted compound FeTe_{1-x}Se_x are relatively large and that a miscible region exists around $x = 0.7 - 0.95$ ³³. Furthermore, the width of B_{1g} mode seems to be much broader for Fe_{1.074}Te. This may be due to the inhomogeneity at the iron sites. As far as characterized by ICP, while the parent compound Fe_{1.074}Te include excess irons, they cannot be detected in the superconducting FeTe_{0.6}Se_{0.4}.

B. Two-magnon Raman Scattering

Figure 5 shows Raman spectra of Fe_{1.074}Te in the wider-energy region up to 7000 cm^{-1} ($\sim 870 \text{ meV}$). Broad peak structures have been observed in all the configurations at $\sim 2300 \text{ cm}^{-1}$ ($\sim 285 \text{ meV}$). Furthermore,

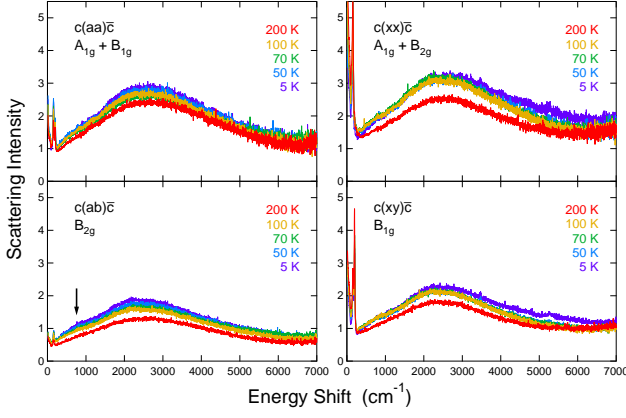


FIG. 5: (Color online) Temperature-dependent Raman spectra of $\text{Fe}_{1.074}\text{Te}$ with the wider-energy region up to 7000 cm^{-1} . Broad peak structures around 2300 cm^{-1} is assigned to the two-magnon excitation. Broad weak edge structures around $300\text{--}800 \text{ cm}^{-1}$ observed below T_s are denoted by the arrow in the (ab) configuration spectra and are considered to be related to the magnetic transition.

broad weak edge structures seem to evolve around $300\text{--}800 \text{ cm}^{-1}$ ($37\text{--}99 \text{ meV}$) below T_s as denoted by the arrow in the (ab) configuration spectra of Fig. 5. We have assigned the broad peak structures around 2300 cm^{-1} to the two-magnon scattering and the weak edge structures to the excitation related to the magnetic transition. In the Raman spectra of BaFe_2As_2 (Ba122), similar broad peak and weak edge structures have been observed.^{36,37} The weak edge structures evolve below the spin-density-wave (SDW) transition temperature T_{SDW} around 400 and 800 cm^{-1} for Ba122. In the optical conductivity $\sigma(\omega)$ of Ba122, also, double-peak structures develop below T_{SDW} and this feature is considered to be related to the SDW gap.³⁸ On the other hand, SDW gap has not been observed in $\sigma(\omega)$ of $\text{Fe}_{1.05}\text{Te}$.³⁹ However, $\sigma(\omega)$ of $\text{Fe}_{1.05}\text{Te}$ shows a prominent temperature dependence below 500 cm^{-1} below T_s . The edge structure around $300\text{--}800 \text{ cm}^{-1}$ in the Raman spectra of $\text{Fe}_{1.074}\text{Te}$ also should be related to the magnetic transition.

The energy of two-magnon scattering is also similar between $\text{Fe}_{1.074}\text{Te}$ and Ba122.^{36,37} This may be surprising at first glance, because the magnetic structure is different between $\text{Fe}_{1.074}\text{Te}$ and Ba122. While Ba122 has a single-stripe AFM structure with the AFM wavevector $\mathbf{Q}_{AF} = (\pi, \pi)$, Fe_{1+y}Te has a double-stripe AFM structure with $\mathbf{Q}_{AF} = (\delta\pi, 0)$. It is natural that one can expect different magnetic interactions from the different AFM structures. In the single-stripe AFM structure, there are two kinds of the first-nearest-neighbor exchange interactions, the AFM interaction J_{1a} and the ferromagnetic (FM) interaction J_{1b} . The second-nearest-neighbor interaction is only one kind of J_2 . On the other hand, in the double-stripe AFM structure, the second-nearest-neighbor interaction is also two kinds, the AFM interaction J_{2a} and

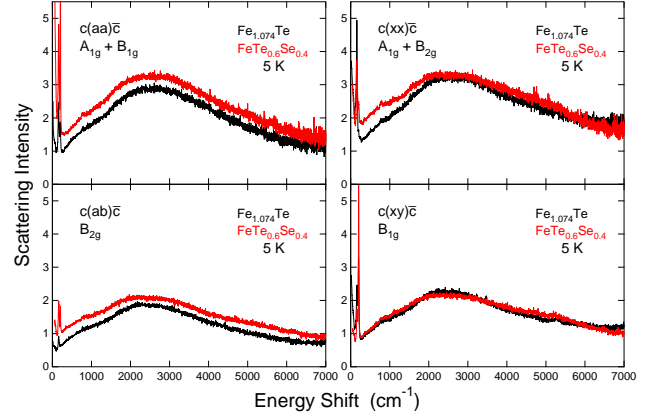


FIG. 6: (Color online) Comparison of two-magnon spectra between the parent compound $\text{Fe}_{1.074}\text{Te}$ and the superconducting $\text{FeTe}_{0.6}\text{Se}_{0.4}$.

the FM interaction J_{2b} . These notations are according to Han *et al.*^{40,41} They have estimated exchange interactions of various iron-based superconductors. Experimentally, Zhao *et al.* have confirmed that the maximum spin-wave bandwidth of Ca122 is $\sim 200 \text{ meV}$ by the INS measurements and deduced the exchange parameters $SJ_{1a} = 49.9 \text{ meV}$, $SJ_{1b} = -5.7 \text{ meV}$, $SJ_2 = 18.9 \text{ meV}$.⁴² These values are qualitatively in agreement with estimation by Han *et al.*⁴⁰ Also, the one-magnon energy can be approximately estimated by energy difference between the ordered state and the excited state with the one spin rotated toward the opposite direction. In the single-stripe AFM structure, the one-magnon energy can be estimated as $2S(J_{1a} - J_{1b} + 2J_2)$ and this corresponds to 186.8 meV using the exchange parameters deduced by the INS measurements and roughly in agreement with the maximum one-magnon energy of the INS measurements. On the other hand, the two-magnon energy can be estimated by energy difference between the ordered state and the excited state with the two neighbor opposite spins rotated toward the each opposite directions, because the total spin quantum number should be conserved by the Raman scattering. Although there are two kinds of the two neighbor spins with the opposite directions in the single-stripe AFM structure, if we assume that the two-magnon excitation energy can be estimated by the minimum value of the energy difference between the two states, it can be estimated as $4S(J_{1a} - J_{1b} + 2J_2) - J_{1a}$ and this corresponds to 323.7 meV by supposing $S = 1$.

For the case of 11 system, the exchange interactions have been estimated as $SJ_{1a} = -7.6 \text{ meV}$, $SJ_{1b} = -26.5 \text{ meV}$, $SJ_{2a} = 46.5 \text{ meV}$, and $SJ_{2b} = -34.9 \text{ meV}$ for the double-stripe $\text{Fe}_{1.068}\text{Te}$ by Han *et al.*⁴¹ based on the first-principle calculations. As the above approximate estimation, the one-magnon and two-magnon energy in the double-stripe AFM structure can be estimated as $2S(J_{1a} - J_{1b} + J_{2a} - J_{2b})$ and $4S(J_{1a} - J_{1b} + J_{2a} - J_{2b}) - J_{2a}$,

respectively, and these values correspond to 200.6 meV and 354.7 meV, respectively. The observed two-magnon peak is somewhat smaller than this estimated value. However, the peak energy of the two-magnon scattering can be smaller than the estimated value from the one-magnon energy because it depends on the details of magnon dispersion relations. Hence, we can say that the peak energy of the two-magnon scattering is reasonable and it is also reasonable that two-magnon energies are similar between $\text{Fe}_{1.074}\text{Te}$ and Ba122 . From the INS measurements of superconducting and non-superconducting $\text{FeTe}_{1-x}\text{Se}_x$, it is insisted that the spin excitation spectrum extends above 250 meV by Lumsden *et al.*⁴³

Figure 6 shows a comparison of the two-magnon spectra between the parent compound $\text{Fe}_{1.074}\text{Te}$ and the superconducting $\text{FeTe}_{0.6}\text{Se}_{0.4}$. One can see that the two-magnon spectra are almost the same between these two compounds. This is rather surprising because $\text{FeTe}_{0.6}\text{Se}_{0.4}$ no longer shows long-range magnetic ordering. For the case of the hole-doped high- T_c cuprates, while the two-magnon peak of the AF parent compounds is relatively sharp in the B_{1g} spectra, it becomes broader and the peak energy becomes smaller with hole doping.⁴⁴ However, because Se substitution is isovalent doping and the parent compound $\text{Fe}_{1.074}\text{Te}$ is an itinerant antiferromagnet, while the parent compound of the high- T_c cuprates is an antiferromagnetic insulator, it may be reasonable that doping dependence is so different from the cuprates. Anyway from these results, we can say that almost the same magnetic excitations and/or magnetic fluctuations exist even in the superconducting $\text{FeTe}_{0.6}\text{Se}_{0.4}$ with the antiferromagnetic $\text{Fe}_{1.074}\text{Te}$.

As for the selection rule of the two-magnon scattering, if the ordered magnetic moments are originated from the localized spins and Hamiltonian of the system can be described by the Heisenberg model including only the nearest neighbor exchange interactions, the two-magnon scattering Hamiltonian can be given by⁴⁵

$$H^{2\text{-mag}} = A \sum_{\langle ij \rangle} (\mathbf{E}_{inc} \cdot \boldsymbol{\sigma}_{ij})(\mathbf{E}_{sc} \cdot \boldsymbol{\sigma}_{ij})(\mathbf{S}_i \cdot \mathbf{S}_j),$$

where \mathbf{E}_{inc} , \mathbf{E}_{sc} are polarization vectors of the incident and scattered light, respectively, $\boldsymbol{\sigma}_{ij}$ is a unit vector connecting the nearest neighbor sites i and j , and \mathbf{S}_i , \mathbf{S}_j are spin operators at the site i and j , respectively. Even using this Hamiltonian, the selection rule can be varied when the crystal and magnetic structures are different. In addition, when not only the nearest neighbor interactions but also further interactions exist, the selection rule can be complex. At least, when the second nearest neighbor interactions are finite, the two-magnon scattering should be active in B_{1g} and B_{2g} mode. In this case, two-magnon scattering can be observed in all our polarization configurations. However, for the case of the iron-based superconductors, since the electric resistivity of parent compounds are metallic, it should not have been settled whether the localized spins exist or not⁴². Hence, the above selection rule might not be applied to

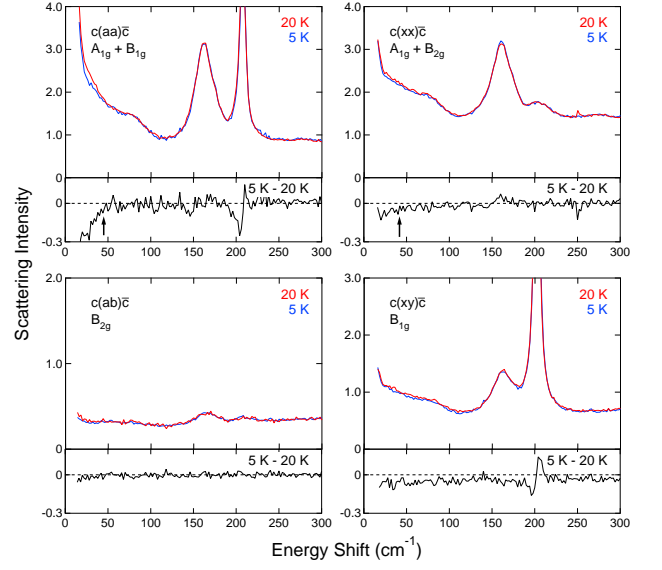


FIG. 7: (Color online) Electronic Raman spectra of $\text{FeTe}_{0.6}\text{Se}_{0.4}$ above and below T_c and difference spectra. Dip structures are denoted by the arrows in the (aa) and (xx) configuration spectra.

the present system. Anyway, we consider that it would be intrinsic that the two-magnon peak has been observed for all our polarization configurations.

C. Electronic Raman Scattering

Finally, we would like to show the spectra of the electronic Raman scattering. Figure 7 shows the Raman spectra in the low-energy region measured below T_c (5 K) and above T_c (20 K), and the difference spectra between these two spectra. Scattering intensity below 100 cm^{-1} should be contributed from the electronic scattering. Because the intensity of the electronic Raman scattering is proportional to the square of the inverse effective-mass tensor $|\frac{m}{\hbar^2} \partial^2 \epsilon / \partial k_\alpha \partial k_\beta|^2$,⁴⁷ the momentum dependence of Raman scattering intensity can be complex for the case of the multiband system like iron-based superconductors. We have calculated the Raman form factor for each polarization configuration based on the unfolded 5-band tight-binding (TB) model reproduced from Ref. 20. Fermi level (E_F) has been shifted to reproduce three hole FS observed by the ARPES measurements of $\text{Fe}_{1.04}\text{Te}_{0.66}\text{Se}_{0.34}$ ⁴⁶ as shown in Fig. 8 (b). Although the parameters of this TB model is evaluated from the first-principle band-structure calculation of $\text{LaFeAsO}_{1-x}\text{F}_x$, the curvatures of each band around E_F are approximately the same as those of the first-principle calculations for FeTe .¹⁴ This has been also confirmed by comparison with our own calculation results with the Quantum-Espresso code. The calculated mo-

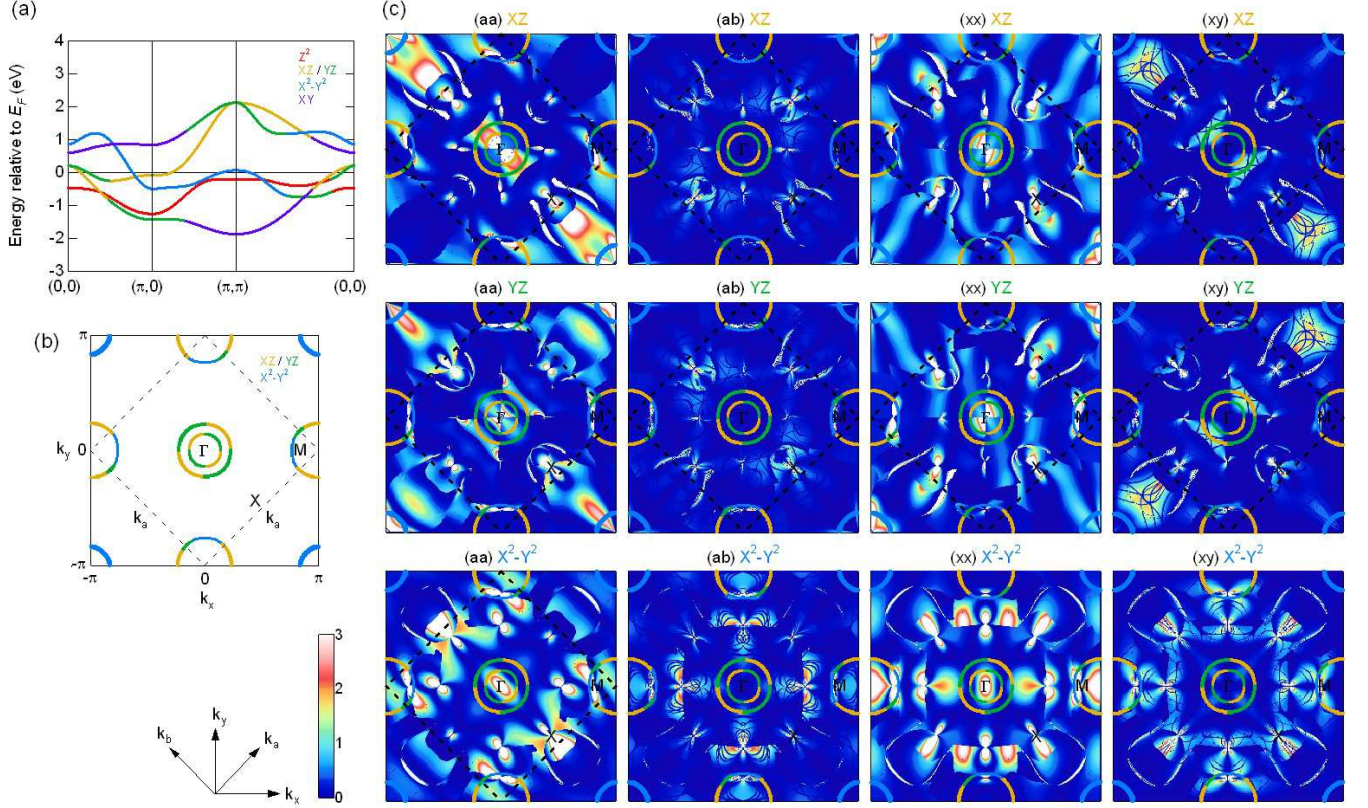


FIG. 8: (Color online) The band structure of the unfolded 5-band tight-binding model reproduced from Ref. 20. Colors are distinguished by the contributions of each orbital. Fermi level has shifted to reproduce three hole FS observed by ARPES.⁴⁶ (b) Fermi surfaces deduced from the 5-band tight-binding model. (c) The top, middle, and bottom panels show the Raman form factors $|\frac{m}{\hbar^2} \partial^2 \epsilon / \partial k_\alpha \partial k_\beta|^2$ of all the measured polarization configurations for the XZ, YZ and X^2-Y^2 bands, respectively. The contributions to the electronic Raman scattering is significant at the white or red regions overlapped with each FS sheet represented by the yellow (XZ band), green (YZ band), and blue (X^2-Y^2 band) lines, respectively.

momentum dependence of the electronic-Raman-scattering intensity is shown in Fig. 8 (c). Because only the XZ, YZ and X^2-Y^2 bands cross the E_F , we have shown only these three bands. One can recognize that the electronic Raman scattering is intense for the (aa) and (xx) polarization, and that relatively large contributions are from the inner XZ/YZ hole FS around (0,0) point and the electronic FS around $(\pi,0)$ point for both configurations. However, we must note that A_{1g} spectra can be partially screened by the long-range Coulomb interactions.⁴⁷ In the difference spectra shown in Fig 7, dip structures around 40-45 cm^{-1} ($= 5.0\text{-}5.6$ meV) can be recognized for (aa) and (xx) configurations as denoted by the arrows. These dip structures can be attributed to decrease of density of states at E_F below T_c . Although the pair-breaking peak has not been observed, which is probably because T_c is too low to be observed by our measurements, if we assume that the dip positions corresponds to 2Δ , this gives a reduced gap value $2\Delta/k_B T_c = 4.0\text{-}4.5$. These values are slightly larger than the reported value from the STS measurements,⁴⁸ but our estimation of 2Δ should be only able to give the upper limit of this

value. It is consistent with the s_{\pm} symmetry of the superconducting gap that the dip structure can be observed in the (aa) and (xx) polarizations, because in these polarizations, the excitations of A_{1g} symmetry can be observed. Hence, we have concluded that these temperature and polarization dependence of the electronic Raman spectra is consistent with the STM/STS results.^{31,48}

Recently, electronic Raman scattering of $\text{Ba}(\text{Fe}_{1-x}\text{Co}_x)_2\text{As}_2$ has been reported^{36,49} and a clear pair breaking peak has been observed for B_{2g} spectrum. Muschler *et al.* have insisted that the B_{2g} spectrum mainly probes the electronic FS around M point, while the A_{1g} spectrum has the largest contribution from the interband scattering involving the hole bands. On the other hand, Sugai *et al.* have proposed that the pairing symmetry of orbital combination is B_{2g} and that of momentum space is A_{1g} . Mazin *et al.* have calculated the symmetry dependent electronic Raman scattering based on the first-principles calculations⁵⁰. This difference between 122 system and 11 system would be originated from the difference of band structures. Mazin *et al.* have pointed out that the band structure of

122 system is more three-dimensional (3D) than other iron-based superconductors. They also have pointed out that because the crystallographic symmetry of 122 system is body-centered tetragonal (bct) and different from other iron-based superconductors, which have primitive tetragonal structures, band folding from the unfolded Brillouin zone is rather complex. Furthermore, because $\text{Ba}(\text{Fe}_{1-x}\text{Co}_x)_2\text{As}_2$ is an electron-doped system while $\text{FeTe}_{1-x}\text{Se}_x$ is an isovalent-doping system, the size of FSs also should be rather different. From these reasons, the superconducting gap may be observed in the different symmetries between $\text{Ba}(\text{Fe}_{1-x}\text{Co}_x)_2\text{As}_2$ and $\text{FeTe}_{1-x}\text{Se}_x$.

V. CONCLUSION

In summary, we have observed the phonon, two-magnon, and electronic Raman scattering of the iron-based superconductor $\text{FeTe}_{1-x}\text{Se}_x$. The A_{1g} and B_{1g} phonon modes at 5 K have been observed at 158 cm^{-1} and 202 cm^{-1} , respectively, for the parent compound $\text{Fe}_{1.074}\text{Te}$ and at 161 cm^{-1} and 202 cm^{-1} , respectively, for the superconducting $\text{FeTe}_{0.6}\text{Se}_{0.4}$. These modes have been assigned to *c*-axis anti-phase vibration modes of the chalcogens and irons, respectively. The frequencies of the observed phonons are reasonably in accord with the calculated results. Two-magnon scattering has been ob-

served as broad peak structures around 2300 cm^{-1} ($\sim 285\text{ meV}$) and the broad weak edge structure around $300\text{--}800\text{ cm}^{-1}$ ($\sim 93\text{ meV}$) has been observed below the magnetic and structural transition temperature T_s ($= 57\text{ K}$) in the spectra of the parent compound. The broad weak edge structure observed below T_s is considered as associated to the magnetic transition. We have estimated the two-magnon energy as $4S(J_{1a} - J_{1b} + J_{2a} - J_{2b}) - J_{2a}$, which corresponds to 354.7 meV using the theoretically estimated values of exchange interactions. The observed two-magnon peak is somewhat smaller than the estimated value. However, because the peak energy of the two-magnon scattering depends on the details of magnon dispersion relations, we have concluded that the observed two-magnon excitation energy is reasonable. In the spectra of the superconducting compound $\text{FeTe}_{0.6}\text{Se}_{0.4}$, also, almost the same two-magnon spectra have been observed. This is rather surprising because $\text{FeTe}_{0.6}\text{Se}_{0.4}$ no longer has a long-range magnetic ordering. This indicates that almost the same magnetic excitations and/or magnetic fluctuations exist even in the superconducting $\text{FeTe}_{0.6}\text{Se}_{0.4}$ with the antiferromagnetic $\text{Fe}_{1.074}\text{Te}$. The difference of the electronic Raman spectra between below T_c (5 K) and above T_c (20 K) has been deduced and dip structures around $40\text{--}45\text{ meV}$ ($= 5.0\text{--}5.6\text{ meV}$) for (aa) and (xx) configurations. This means that the superconducting gap has a A_{1g} symmetry and consistent with the STM/STS results.

-
- * Present address: Institute for Solid State Physics, University of Tokyo, Kashiwa, Chiba 277-8581, Japan; Electronic address: okazaki@issp.u-tokyo.ac.jp
- ¹ Y. Kamihara, T. Watanabe, M. Hirano, and H. Hosono, *J. Am. Chem. Soc.* **130**, 3296 (2008).
 - ² H. Takahashi, K. Igawa, K. Arii, Y. Kamihara, M. Hirano, and H. Hosono, *Nature* **453**, 376 (2008), ISSN 0028-0836.
 - ³ Z.-A. Ren, J. Yang, W. Lu, W. Yi, X.-L. Shen, Z.-C. Li, G.-C. Che, X.-L. Dong, L.-L. Sun, F. Zhou, et al., *Chinese Physics Letters* **25**, 2215 (2008).
 - ⁴ M. Rotter, M. Tegel, D. Johrendt, I. Schellenberg, W. Hermes, and R. Pöttgen, *Phys. Rev. B* **78**, 020503 (2008).
 - ⁵ M. Rotter, M. Tegel, and D. Johrendt, *Phys. Rev. Lett.* **101**, 107006 (2008).
 - ⁶ J. H. Tapp, Z. Tang, B. Lv, K. Sasmal, B. Lorenz, P. C. W. Chu, and A. M. Guloy, *Phys. Rev. B* **78**, 060505 (2008).
 - ⁷ X. Wang, Q. Liu, Y. Lv, W. Gao, L. Yang, R. Yu, F. Li, and C. Jin, *Solid State Communications* **148**, 538 (2008).
 - ⁸ F.-C. Hsu, J.-Y. Luo, K.-W. Yeh, T.-K. Chen, T.-W. Huang, P. M. Wu, Y.-C. Lee, Y.-L. Huang, Y.-Y. Chu, D.-C. Yan, et al., *Proc. Natl. Acad. Sci. U.S.A.* **105**, 14262 (2008).
 - ⁹ K.-W. Yeh, T.-W. Huang, Y. Lin Huang, T.-K. Chen, F.-C. Hsu, P. M. Wu, Y.-C. Lee, Y.-Y. Chu, C.-L. Chen, J.-Y. Luo, et al., *Europhys. Lett.* **84**, 37002 (2008).
 - ¹⁰ M. H. Fang, H. M. Pham, B. Qian, T. J. Liu, E. K. Vehstedt, Y. Liu, L. Spinu, and Z. Q. Mao, *Phys. Rev. B* **78**, 224503 (2008).
 - ¹¹ X. Zhu, F. Han, G. Mu, P. Cheng, B. Shen, B. Zeng, and H.-H. Wen, *Phys. Rev. B* **79**, 220512 (2009).
 - ¹² D. J. Singh and M.-H. Du, *Phys. Rev. Lett.* **100**, 237003 (2008).
 - ¹³ D. J. Singh, *Phys. Rev. B* **78**, 094511 (2008).
 - ¹⁴ A. Subedi, L. Zhang, D. J. Singh, and M. H. Du, *Phys. Rev. B* **78**, 134514 (2008).
 - ¹⁵ G. Wang, M. Zhang, L. Zheng, and Z. Yang, *Phys. Rev. B* **80**, 184501 (2009).
 - ¹⁶ J. Dong, H. J. Zhang, G. Xu, Z. Li, G. Li, W. Z. Hu, D. Wu, G. F. Chen, X. Dai, J. L. Luo, et al., *Europhysics Letters* **83**, 27006 (2008).
 - ¹⁷ G. Xu, H. Zhang, X. Dai, and Z. Fang, *Europhysics Letters* **84**, 67015 (2008).
 - ¹⁸ S. Deng, J. Köhler, and A. Simon, *Phys. Rev. B* **80**, 214508 (2009).
 - ¹⁹ I. I. Mazin, D. J. Singh, M. D. Johannes, and M. H. Du, *Phys. Rev. Lett.* **101**, 057003 (2008).
 - ²⁰ K. Kuroki, S. Onari, R. Arita, H. Usui, Y. Tanaka, H. Kontani, and H. Aoki, *Phys. Rev. Lett.* **101**, 087004 (2008).
 - ²¹ H. Ding, P. Richard, K. Nakayama, K. Sugawara, T. Arakane, Y. Sekiba, A. Takayama, S. Souma, T. Sato, T. Takahashi, et al., *Europhysics Letters* **83**, 47001 (2008).
 - ²² Y. Xia, D. Qian, L. Wray, D. Hsieh, G. F. Chen, J. L. Luo, N. L. Wang, and M. Z. Hasan, *Phys. Rev. Lett.* **103**, 037002 (2009).
 - ²³ C. de la Cruz, Q. Huang, J. W. Lynn, J. Li, W. R. II, J. L. Zarestky, H. A. Mook, G. F. Chen, J. L. Luo, N. L. Wang, et al., *Nature* **453**, 899 (2008).
 - ²⁴ Q. Huang, Y. Qiu, W. Bao, M. A. Green, J. W. Lynn,

- Y. C. Gasparovic, T. Wu, G. Wu, and X. H. Chen, Phys. Rev. Lett. **101**, 257003 (2008).
- ²⁵ S. Li, C. de la Cruz, Q. Huang, Y. Chen, J. W. Lynn, J. Hu, Y.-L. Huang, F.-C. Hsu, K.-W. Yeh, M.-K. Wu, et al., Phys. Rev. B **79**, 054503 (2009).
 - ²⁶ S. Medvedev, T. M. McQueen, I. A. Troyan, T. Palasyuk, M. I. Erements, R. J. Cava, S. Naghavi, F. Casper, V. Ksenofontov, G. Wortmann, et al., Nature Mater **8**, 630 (2009).
 - ²⁷ S. Margadonna, Y. Takabayashi, Y. Ohishi, Y. Mizuguchi, Y. Takano, T. Kagayama, T. Nakagawa, M. Takata, and K. Prassides, Phys. Rev. B **80**, 064506 (2009).
 - ²⁸ S. Margadonna, Y. Takabayashi, M. T. McDonald, K. Kasperkiewicz, Y. Mizuguchi, Y. Takano, A. N. Fitch, E. Suard, and K. Prassides, Chem. Commun. **2008**, 5607 (2008).
 - ²⁹ W. Bao, Y. Qiu, Q. Huang, M. A. Green, P. Zajdel, M. R. Fitzsimmons, M. Zhernenkov, S. Chang, M. Fang, B. Qian, et al., Phys. Rev. Lett. **102**, 247001 (2009).
 - ³⁰ Y. Qiu, W. Bao, Y. Zhao, C. Broholm, V. Stanev, Z. Teseanovic, Y. C. Gasparovic, S. Chang, J. Hu, B. Qian, et al., Phys. Rev. Lett. **103**, 067008 (2009).
 - ³¹ T. Hanaguri, S. Niitaka, K. Kuroki, and H. Takagi, Science **328**, 474 (2010).
 - ³² P. Giannozzi, S. Baroni, N. Bonini, M. Calandra, R. Car, C. Cavazzoni, D. Ceresoli, G. L. Chiarotti, M. Cococcioni, I. Dabo, et al., J. Phys.: Condens. Matter **21**, 395502 (2009).
 - ³³ Y. Mizuguchi, F. Tomioka, S. Tsuda, T. Yamaguchi, and Y. Takano, J. Phys. Soc. Jpn. **78**, 074712 (2009).
 - ³⁴ T.-L. Xia, D. Hou, S. C. Zhao, A. M. Zhang, G. F. Chen, J. L. Luo, N. L. Wang, J. H. Wei, Z.-Y. Lu, and Q. M. Zhang, Phys. Rev. B **79**, 140510 (2009).
 - ³⁵ P. Kumar, A. Kumar, S. Saha, D. Muthu, J. Prakash, S. Patnaik, U. Waghmare, A. Ganguli, and A. Sood, Solid State Commun. **150**, 557 (2010), ISSN 0038-1098.
 - ³⁶ S. Sugai, Y. Mizuno, K. Kiho, M. Nakajima, C. H. Lee, A. Iyo, H. Eisaki, and S. Uchida, Phys. Rev. B **82**, 140504 (2010).
 - ³⁷ S. Sugai, Y. Mizuno, R. Watanabe, T. Kawaguchi, K. Takenaka, H. Ikuta, Y. Takayanagi, N. Hayamizu, and Y. Sone, arXiv:1010.6151v1 (unpublished).
 - ³⁸ W. Z. Hu, J. Dong, G. Li, Z. Li, P. Zheng, G. F. Chen, J. L. Luo, and N. L. Wang, Phys. Rev. Lett. **101**, 257005 (2008).
 - ³⁹ G. F. Chen, Z. G. Chen, J. Dong, W. Z. Hu, G. Li, X. D. Zhang, P. Zheng, J. L. Luo, and N. L. Wang, Phys. Rev. B **79**, 140509 (2009).
 - ⁴⁰ M. J. Han, Q. Yin, W. E. Pickett, and S. Y. Savrasov, Phys. Rev. Lett. **102**, 107003 (2009).
 - ⁴¹ M. J. Han and S. Y. Savrasov, Phys. Rev. Lett. **103**, 067001 (2009).
 - ⁴² J. Zhao, D. T. Adroja, D.-X. Yao, R. Bewley, S. Li, X. F. Wang, G. Wu, X. H. Chen, J. Hu, and P. Dai, Nature Phys. **5**, 555 (2009).
 - ⁴³ M. D. Lumsden, A. D. Christianson, E. A. Goremychkin, S. E. Nagler, H. A. Mook, M. B. Stone, D. L. Abernathy, T. Guidi, G. J. MacDougall, C. de la Cruz, et al., Nature Phys. **6**, 182 (2010).
 - ⁴⁴ S. Sugai, H. Suzuki, Y. Takayanagi, T. Hosokawa, and N. Hayamizu, Phys. Rev. B **68**, 184504 (2003).
 - ⁴⁵ J. B. Parkinson, Journal of Physics C: Solid State Physics **2**, 2012 (1969).
 - ⁴⁶ F. Chen, B. Zhou, Y. Zhang, J. Wei, H.-W. Ou, J.-F. Zhao, C. He, Q.-Q. Ge, M. Arita, K. Shimada, et al., Phys. Rev. B **81**, 014526 (2010).
 - ⁴⁷ T. P. Devereaux and R. Hackl, Rev. Mod. Phys. **79**, 175 (2007).
 - ⁴⁸ T. Kato, Y. Mizuguchi, H. Nakamura, T. Machida, H. Sakata, and Y. Takano, Phys. Rev. B **80**, 180507 (2009).
 - ⁴⁹ B. Muschler, W. Prestel, R. Hackl, T. P. Devereaux, J. G. Analytis, J.-H. Chu, and I. R. Fisher, Phys. Rev. B **80**, 180510 (2009).
 - ⁵⁰ I. I. Mazin, T. P. Devereaux, J. G. Analytis, J.-H. Chu, I. R. Fisher, B. Muschler, and R. Hackl, Phys. Rev. B **82**, 180502 (2010).